

Quantum Dot Size Dependent J – V Characteristics in Heterojunction ZnO/PbS Quantum Dot Solar Cells

Jianbo Gao,^{†,‡} Joseph M. Luther,[†] Octavi E. Semonin,^{†,§} Randy J. Ellingson,[‡] Arthur J. Nozik,^{†,§} and Matthew C. Beard^{1*,†}

[†]Chemical and Material Sciences Center, National Renewable Energy Laboratory, Golden, Colorado 80401, United States

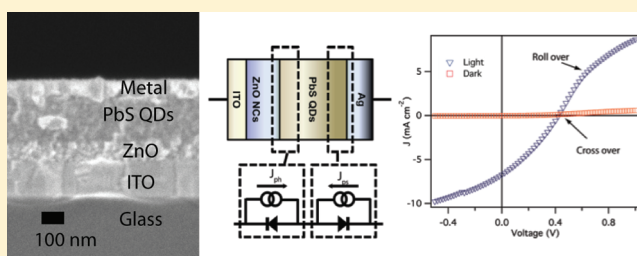
[‡]Department of Physics and Astronomy, Wright Center for Photovoltaics Innovation and Commercialization, University of Toledo, Toledo, Ohio 43606, United States

[§]Department of Chemistry and Biochemistry, University of Colorado at Boulder, Boulder, Colorado 80309, United States

S Supporting Information

ABSTRACT: The current–voltage (J – V) characteristics of ZnO/PbS quantum dot (QD) solar cells show a QD size-dependent behavior resulting from a Schottky junction that forms at the back metal electrode opposing the desirable diode formed between the ZnO and PbS QD layers. We study a QD size-dependent roll-over effect that refers to the saturation of photocurrent in forward bias and crossover effect which occurs when the light and dark J – V curves intersect. We model the J – V characteristics with a main diode formed between the n-type ZnO nanocrystal (NC) layer and p-type PbS QD layer in series with a leaky Schottky-diode formed between PbS QD layer and metal contact. We show how the characteristics of the two diodes depend on QD size, metal work function, and PbS QD layer thickness, and we discuss how the presence of the back diode complicates finding an optimal layer thickness. Finally, we present Kelvin probe measurements to determine the Fermi level of the QD layers and discuss band alignment, Fermi-level pinning, and the V_{oc} within these devices.

KEYWORDS: Quantum Dots, solar cells, heterojunction, double diode, PbS



Schottky-junction quantum dot solar cells (QDSCs) have attracted intense attention in the past few years,^{1–4} but they have several limitations. While large short circuit currents (J_{sc}) of over 20 mA/cm² are achieved, the open circuit voltage (V_{oc}) is low compared to the band gap energy, E_g . The maximum V_{oc} obtainable in a Schottky geometry is likely limited to $E_g/2q$, where q is the charge of an electron. The low V_{oc} 's typically reported are attributed to Fermi-level pinning at the metal/semiconductor junction. Because the Schottky junction forms at the back electrode opposite from where light is incident, minority carriers (electrons) recombine or are trapped at defect sites before they reach the negative electrode. To overcome the above limitations, an “inverted cell” structure can be used, where light is incident upon the high-field region that forms at the heterojunction of a transparent n-type metal oxide layer with the p-type PbS QD layer.^{5–8} Here, minority carriers should flow toward the metal oxide while holes are extracted at the high work function back contact. In this structure, the V_{oc} is determined by the difference in the quasi-Fermi levels in the PbS QD and ZnO layers. We recently reported an NREL-certified ~3% efficient device with structure of ITO/ZnO NC/PbS QD/Au with a V_{oc} that is greater than the PbS bulk band gap, demonstrating that quantum confinement effects can be utilized in QDSCs.⁷ The device is remarkably stable in air without encapsulation for more than 1000 h. However, a full understanding of exciton dissociation

and space charge within the device is lacking. There is ample room for improvement in all three key factors that impact efficiency: J_{sc} , V_{oc} , and fill factor (FF). Here we analyze the size-dependent J – V characteristics and discuss limiting factors of the device architecture with suggested routes for improvement.

We focus on ITO/ZnO NC/PbS QD/metal devices fabricated in air with eight different diameters of PbS QD with first exciton transition energies (effective band gaps) ranging from 0.76 to 2.1 eV. ZnO NC layers were spin coated at 2000 rpm from chloroform onto a cleaned glass substrate with prepatterned ITO electrodes of 150 nm thickness (Thin Film Devices, Anaheim). The resulting ~100 nm thick ZnO layer composed of ~5 nm nanocrystals was heated on a hot plate set to 260 °C for 30 min to remove residual solvent. The PbS QD layer was deposited onto the ZnO layer via sequentially immersing the substrate into a PbS QD hexane solution of concentration 10 mg/mL followed by 1 mM 1,2-ethanedithiol (EDT) in acetonitrile solution.^{1,5,9} Approximately 30 dipping cycles were required to produce QD layer thicknesses of 200–270 nm. The film growth rate is fairly linear with the number of dip cycles and depends primarily on the QD concentration.¹⁰ Au or Ag is

Received: October 29, 2010

Revised: January 4, 2011

Published: February 03, 2011

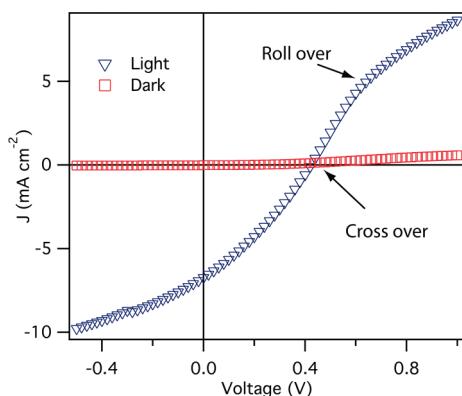


Figure 1. Typical characteristics of J – V in the dark and under 1 sun illumination, which shows the crossover and roll-over effects. The device structure is ITO/ZnO NC/PbS QD/Ag with PbS layer thickness of ~ 550 nm.

evaporated onto the top of the film at a rate of 0.1 nm/s with base pressure of 1×10^{-7} Torr to produce ~ 100 nm layers. All devices are formed with an active area of 0.11 cm² defined by the overlap of the contact electrodes. Synthesis of the ZnO NCs and PbS QDs followed previous published reports,⁵ and more detailed information concerning layer thickness and QD diameters is provided in the Supporting Information.

Figure 1 shows the J – V characteristic of a device with 550 nm thick PbS QD layer with Ag as the back contact. The plot exemplifies the roll-over effect (current saturation at high forward bias) under illumination and the crossover effect (intersection of dark and light current under forward bias). The dark curve is nearly flat while the light curve appears relatively normal in the power quadrant but begins to saturate above the V_{oc} . A hole-injection barrier resulting from a Schottky barrier that forms at the PbS QD/metal interface can explain both of these abnormalities in the J – V response. The roll-over effect, also observed in CdTe thin film^{11,12} and organic solar cells,^{13,14} is due to a back contact hole-injection barrier. The crossover effect is dominant in Cu₂S devices^{15–18} and has been reported recently in QD based devices.¹⁹

A schematic of the PbS QD device is shown in Figure 2a and the two-diode equivalent circuit is shown in Figure 2b with boxes denoting the lumped equivalent circuit for each interface. Figure 2c is a schematic of the equilibrium band diagram. Photogenerated minority carriers in the PbS layer can either be swept into the ZnO layer and transported to the anode or swept into the back metal cathode, thus leading to opposing currents. Holes are majority carriers and, therefore, should be extracted at the metal cathode but experience a hole-injection barrier at both the ZnO and metal interfaces.

J – V Simulations and Schottky Barrier Height. To simulate the solar cell J – V relationship, we employ a commonly used lumped circuit model that includes a diode with diode quality factor, a shunt resistance R_{sh} in parallel with the diode, and a series resistance R_s .^{20,21} The shunt resistance indicates the degree of charges lost due to recombination and trapping, while the series resistor R_s considers conductivity, i.e., mobility of specific charge carrier in the respective transport medium. The J – V characteristics in our case follow a two-diode model with opposing diodes connected in series at the anode. In the following description, the subscript h refers to the heterojunction diode and s refers to the Schottky diode. Under illumination the

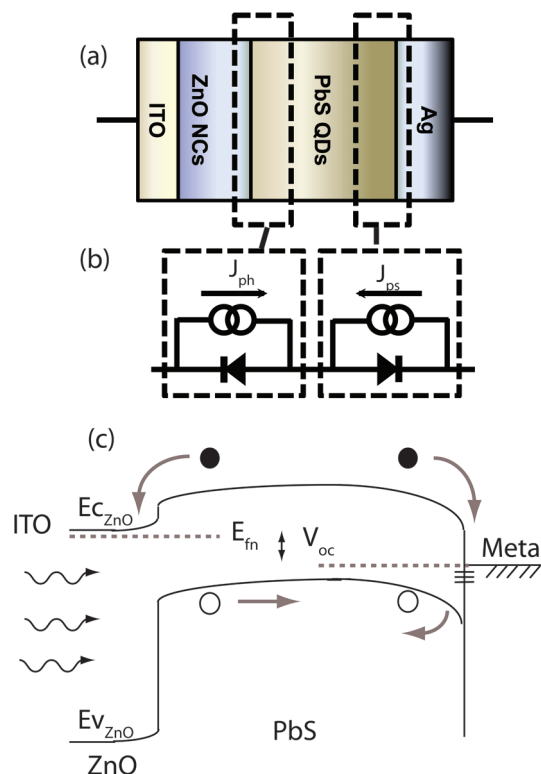


Figure 2. (a) Schematic of the inverted solar cell with structure of ITO/ZnO NC/PbS QD/Ag. (b) Two-diode model equivalent circuit including a heterojunction diode between the ZnO and PbS QD layers and a Schottky junction diode between PbS QD film and Au or Ag. The junctions marked by dashed rectangular lines in panel a schematically indicate the corresponding diodes in panel b. (c) Device band diagram under illumination. Holes meet barrier height at the Ag or Au electrode, and electrons can flow in either of two opposite directions to electrode. (See Supporting Information for an SEM image of a cross section of a device.)

current across the heterojunction diode can be expressed as

$$J_h = J_{ph} - J_{h0} (e^{qV_h/n_h kT} - 1) - V_h/R_{sh,h} \quad (1)$$

where J_{h0} is the saturation current, J_{ph} is the photogenerated current, $R_{sh,h}$ is the heterojunction diode shunt resistance, and n_h is the heterojunction diode ideality factor. The current that flows through the Schottky junction diode is

$$J_s = -J_{ps} + J_{s0} (e^{qV_s/kT} - 1) + V_s/R_{sh,s} \quad (2)$$

where J_{s0} is the saturation current, J_{ps} is the photogenerated current, and $R_{sh,s}$ is the Schottky diode shunt resistance. Because the two diodes are in series, the current is equivalent through each diode, while the applied bias, V , is divided between the heterojunction, V_h , Schottky junction, V_s , and any resistive components, IR_s , therefore

$$V = V_h + V_s + IR_s \quad (3)$$

eqs 1–3 can be solved to generate the J – V characteristics⁹ and are used to model the measured data.

Figure 3 displays illuminated J – V characteristics of devices made from the various PbS QD diameters, with Ag (panel a) and Au (panel b) as the back contact. In the Supporting Information we show an expanded voltage range as well as the dark J – V

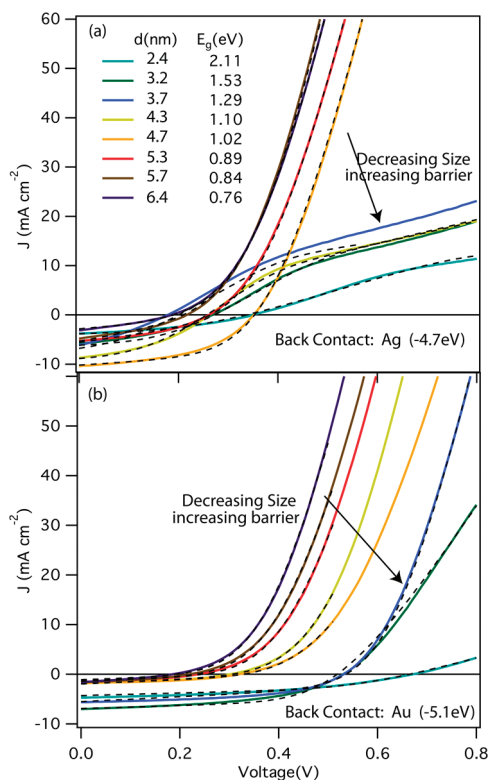


Figure 3. J - V curves for eight devices made from PbS QDs with various diameters. Panel a is for devices with Ag as the back contact and panel b is for Au. Modeled curves are shown as black dotted lines.

curves (Figures S1–S4, Supporting Information). The roll-over effect is obvious for E_g greater than ~ 1 eV and is nearly absent below 1 eV. Similarly, the crossover effect is also most pronounced for band gaps greater 1 eV and diminishes for smaller band gaps. For small QDs with larger band gap,²² the barrier height between the PbS layer and Ag is large enough to block hole-injection; therefore, holes accumulate at the interface, causing the current to saturate. For larger QDs with smaller band gap, the barrier is reduced allowing for some hole injection, which occurs via thermionic emission. The barrier height can also be reduced if Au replaces Ag. The J - V characteristics with Au as the back contact are shown in Figure 3b, because of the lower work function the transition from normal J - V curves to ones that exhibit roll-over and crossover occurs for effective band gaps greater than ~ 1.4 eV. While some J - V curves do not exhibit roll-over, almost all exhibit crossover; however, crossover is most pronounced for the J - V curves that exhibit roll-over. Note that even for J - V curves that do not exhibit roll-over, the back Schottky junction can limit device performance.²³

We model the J - V curves for both Au and Ag back contact devices using eqs 1–3. The results of a nonlinear least-squares fitting routine are shown as black dotted lines in Figure 3. The dark J - V curves were modeled simultaneously with the light curves and the dark J - V results are shown in Figures S2 and S4 (Supporting Information) as the black dotted lines. The extracted parameters are tabulated in Tables S2 and S3 of the Supporting Information. Previous reports show how the Schottky-junction barrier height formed by PbS QD films depends on the contact work function and QD size.^{1–4} The current at which roll-over occurs is determined by the Schottky saturation current, J_{so} . In Figure 4, we plot the extracted values for J_{so} and $J_{ph,h}$ as a

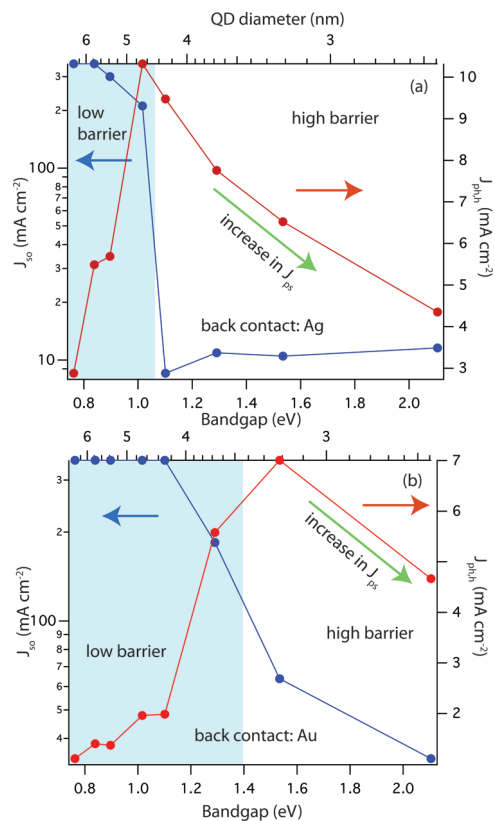


Figure 4. Extracted values of the photocurrent (red circles) and Schottky-barrier saturation current (blue circles) for devices with (a) Ag as back contact and (b) Au.

function of band gap energy. The extracted photocurrent, $J_{ph,h}$ is the sum of the photocurrent generated by the heterojunction minus the photocurrent generated by the Schottky junction, while J_{so} is related to the Schottky-barrier height by the following relationship¹⁰

$$J_{so} = qn_v v_R e^{-q\phi_b/kT} \quad (4)$$

where n_v is the effective density of valence band states, v_R is the thermal velocity of carriers, and ϕ_b is the Schottky barrier height. A large J_{so} indicates a poor Schottky junction. From eq 4, ϕ_b is inversely related to J_{so} . In accordance with our observations discussed above, J_{so} is high for smaller band gap QDs (larger size) and is lower for higher band gap QDs (smaller size); see Figure 4. For Ag devices, J_{so} undergoes a transition from high to low at $E_g \sim 1.1$ eV while for the Au devices the transition occurs at $E_g \sim 1.4$ eV. The blue shaded areas in Figure 4 represent the low-barrier region, and the unshaded areas are the high-barrier region. The extracted photocurrent, $J_{ph,h}$ exhibits interesting trends and is correlated to the high- or low-barrier regimes. For the high barrier regime, $J_{ph,h}$ decreases from a maximum at the interface between the high and low barrier regimes as the QD size decreases and the barrier-height increases. This is likely due to a combination of increasing photocurrent generated at the Schottky junction that opposes the main heterojunction current and decreased light absorption as the band edge of the QD layer is blue-shifted. Simulations of light absorption¹⁰ within these types of devices indicate that light absorbed near the back electrode (within ~ 100 nm) is roughly constant with change in QD diameter, while light absorbed within ~ 100 nm of the ZnO/PbS interface decreases for

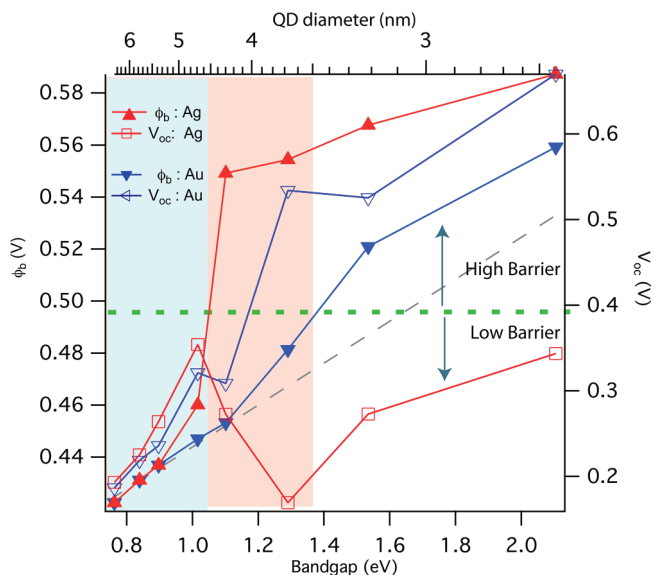


Figure 5. V_{oc} (open red squares correspond to Ag and open blue triangles to Au) and ϕ_b (filled red triangles correspond to Ag and filled blue triangles to Au) dependence with PbS QD band gap energy (QD diameter is shown on the top axis). A straight gray dotted line is drawn to extend the ϕ_b band gap dependence to larger band gaps and illustrates where the measured ϕ_b deviates. The horizontal green dashed line is drawn at ~ 0.5 V and indicates the transition from low to high barrier.

smaller QD diameters. Therefore, the decrease in $J_{ph,h}$ is a combination of decreased light absorption near the ZnO/PbS interface and strengthening of the Schottky barrier and therefore increased carrier extraction that opposes the current extraction from the heterojunction. In the low barrier regime, $J_{ph,h}$ decreases for smaller E_g . This is likely due to a weakening of the heterojunction's electric field resulting in lower carrier extraction and increased carrier recombination, but further work is required in order to understand why $J_{ph,h}$ decreases in this regime.

To calculate ϕ_b we need to estimate v_R and n_v . In bulk semiconductors the thermal velocity of carriers is, $v_R = 1/2\pi \cdot (kT/m^*)^{1/2}$ and for simplicity we assume that $m^* = 1$; therefore, $v_R = 2.69 \times 10^7$ cm/s. The effective density of valence band edge states, n_v , can be estimated by assuming that each QD can provide at most eight states at the band edge. The band gap in PbS occurs at the four equivalent L-points of the Brillouin zone and is therefore 8-fold degenerate.^{24,25} We assume QDs are randomly packed and are touching; therefore, the fill fraction is at most 0.56,²⁶ and the effective volume that each QD occupies is $V_{eff} = V_{QD}/0.56$ and $n_v = 8/V_{eff}$. In Figure S6 (Supporting Information) we plot n_v as a function of QD diameter and then estimate ϕ_b using eq 4 and plot the results along with the measured V_{oc} in Figure 5. While n_v is only estimated here, the value of ϕ_b depends on the $\ln(n_v)$ and, therefore, depends weakly on our estimation.

The low-to-high ϕ_b transition is consistent with trends in V_{oc} . For QDs with E_g less than 1.1 eV, the V_{oc} is identical for Au and Ag back contacts consistent with the idea that for these sized QDs, the back contact forms an Ohmic contact. For smaller diameters the V_{oc} is higher for Au compared to Ag. In particular, for E_g greater than 2 eV, the V_{oc} reaches 670 mV with Au contacts versus 350 mV with Ag. The barrier-heights, ϕ_b for the Au and Ag back contact devices are nearly identical for QD band gap energies less than 1 eV and increases with increasing band gap

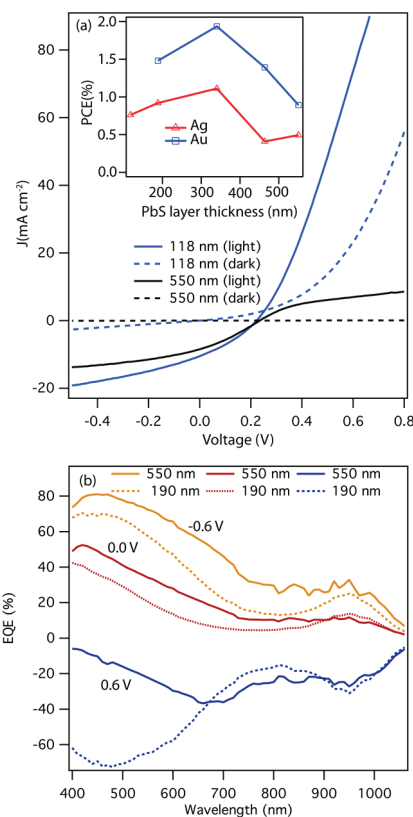


Figure 6. (a) J – V characteristics of devices structure ITO/ZnO NC/PbS QD/Ag under 1 sun illumination with two PbS layer thicknesses, the black lines correspond to 550 nm and the blue lines to 118 nm. The dash lines are for the dark J – V curves. The PbS QD size is 3.7 nm. The inset is power conversion efficiency (PCE) as a function of PbS QD layer thickness with top contact of Au (blue) and Ag (red). (b) EQE spectra of various thickness PbS layers under different bias. The EQE is defined as the dark – light so that under reverse bias the EQE is positive as described in the text.

energy. A nearly straight line indicating an increasing ϕ_b with increasing band gap energy is found for devices consisting of QD band gap energies between 0.6 and 1.1 eV. We have drawn in a straight line (shown as the dotted gray line) that extends this trend to smaller QDs and is consistent with an increasing n_v (Figure S6, Supporting Information) for the smaller QDs. ϕ_b deviates from the line at different QD diameters depending on the back contact. ϕ_b values for the Ag device deviate at E_g of 1.1 eV, represented by the shaded blue region, while ϕ_b for the Au device deviates at E_g of ~ 1.4 eV, represented by the shaded red region. ϕ_b increases above the dashed line for both the Au and Ag devices. The midpoint of the transition from a low barrier to high barrier is ~ 0.5 V, and a horizontal dashed line is drawn indicating the transition from low to high barrier. This is roughly consistent with the low to high barrier transition found for CdTe devices.²³ The band gap at which the transitions occurs is ~ 1.1 eV for the Au back contact devices and ~ 1.4 eV for Ag, and the difference is approximately equal to the difference in the work function of Ag and Au (4.7 and 5.1 eV). Finally, the size-dependent series resistance, R_s (Figure S5, Supporting Information), increases for smaller QDs consistent with recent FET mobility measurements for PbSe EDT treated films which found that the mobility increased for larger QDs.²⁷

Layer Thickness Dependence. To investigate the behavior of the two diodes, Figure 6a shows $J-V$ characteristics with two different layer thicknesses (118 and 550 nm) and Ag as the back contact. The 118 nm device does not exhibit significant roll-over in contrast to the 550 nm device; however, both exhibit cross-over. In CdTe thin film solar cells, the absorber thickness is larger than the minority carrier diffusion length; therefore, one can reasonably assume that the main and the back diodes are independent circuit elements with little interaction. For reasonably thick CdTe ($>3 \mu\text{m}$), the conduction and valence bands are flat over much of the CdTe thickness.^{13,14} In our case, the PbS QD layer thickness is thin relative to ~ 150 nm reported depletion region at the PbS QD/Ag interface.¹ Thus, it is likely that the two diodes interact, and one possible consequence is that the main diode may override the Schottky junction lowering the hole-injection barrier but at the same time reducing the efficiency of the main diode.²⁸ Other possible consequences of this interaction need further study. The presence of the back diode complicates the ability to optimize these devices. The power conversion efficiency as a function of PbS layer thickness is shown in the inset to Figure 6a. The optimal thickness is ~ 340 nm for both Au and Ag contacts. For thicknesses less than ~ 340 nm, the efficiency decreases due to decreasing light absorption while for thicknesses greater 340 nm the efficiency decreases due to strengthening of the back diode.

Further insight can be gained from bias-dependent external quantum efficiency (EQE) measurements shown in Figure 6b. The EQE is measured using a lock-in amplifier synchronized to an optical chopper that modulates the incident light. The phase of the lock-in amplifier is adjusted so that the measured EQE is positive under zero bias and corresponds to the dark current minus the light current; therefore, under forward bias, where the light and dark curves have crossed, the EQE becomes negative. Under negative and zero bias, the EQE spectra have similar shapes for both thin and thick layers, where the EQE is higher in the thicker layer due to increased light absorption. However, under positive bias and for wavelengths less than ~ 650 nm, the EQE spectra deviate from one another. Blue photons generate holes near the PbS/ZnO interface and they must transport across the entire layer prior to recombination. Longer wavelength photons, greater than ~ 650 nm, penetrate further into the film and generate carriers near both contacts. These results indicate that carriers generated near the PbS/ZnO interface experience the back diode differently than carriers generated throughout the film. A plausible explanation is that photo-generated carriers near the Schottky junction decrease the effective hole injection barrier.

Fermi Level Measurements. We employ Kelvin probe measurements to determine the Fermi level of the PbS and ZnO NC layers. Kelvin probe measurements determine the position of the Fermi level relative to a reference surface, and for these measurements a stainless steel standard is used as the reference with work function values of ca. -4.2 to -4.3 eV measured by ultraviolet photoelectron spectroscopy (UPS). We plot the relative values of the Fermi level in Figure 7 (light blue squares are for the PbS QD layers and the brown dashed line is for ZnO). From the relative values of the PbS Fermi level we determined the relative position of the valence band, $E_v'(\text{PbS})$, by the following relationship

$$E_v'(\text{PbS}) = E_f'(\text{PbS}) + kT \ln(p/n_v)$$

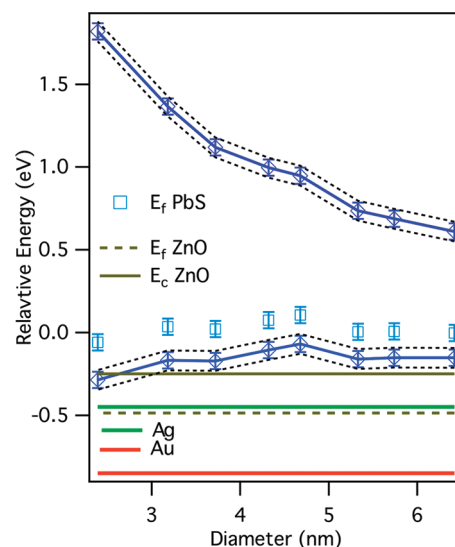


Figure 7. (a) Band positions relative to a stainless steel standard for EDT treated PbS QD layers, ZnO NCs, and the work functions of Au and Ag. The conduction and valence bands for the PbS QDs (blue triangles) are determined from the value of the Fermi energy determined from Kelvin probe measurements (light blue squares). The Fermi level of the ZnO NCs (brown dashed line) was determined from the Kelvin probe measurements and the ZnO conduction band edge, and work functions of the Au and Ag were taken from literature values.

where p is the effective hole doping density of the PbS QD layers and we assume $p = 1 \times 10^{17} \text{ cm}^{-3}$,¹ and n_v is the effective density of valence band states (Figure S6, Supporting Information). The relative conduction band position, $E_c'(\text{PbS})$, is determined by adding the band gap energy to the valence band (shown as blue triangles in Figure 7a). The black dotted lines in Figure 7a show the $E_c'(\text{PbS})$ and $E_v'(\text{PbS})$ for a doping density of $p = 1 \times 10^{16}$ and $p = 1 \times 10^{18} \text{ cm}^{-3}$. We also show literature values adjusted for the reference work function for the conduction band of the ZnO, $E_c(\text{ZnO})$, and the work functions of the Au and Ag. The absolute values of $E_c(\text{PbS})$ and $E_v(\text{PbS})$ differ from a recent report using cyclic voltammetry (CV),²⁹ but we can recover those results by shifting our values by a constant amount depending on the value of the reference work function. The differing results may be due to a difference between CV and Kelvin probe measurements, or the chemical treatment used to produce conductive films may shift the bands. In a UPS study, Timp and Zhu³⁰ report that the valence band of EDT treated PbSe QD films on ZnO are shifted by $0.1-0.3$ eV, depending on the QD size relative to a hydrazine treatment. They suggest that the Fermi level of the QDs is pinned to ZnO surface states. A similar effect may occur here, and further investigations are underway.

Our results, which are independent of the reference work function, imply that EDT treated PbS QD layers will always form a type II interface with ZnO irrespective of the QD diameter. This is in contrast to what has been reported for PbSe/ZnO interfaces where a transition from type I for larger QDs to type II for smaller QDs occurs.²² Because the Fermi level of the ZnO NC layer is lower than that of the PbS QD layers, an unfavorable equilibrium band alignment should occur at this interface. Furthermore, the work functions of Au and Ag are larger than the Fermi level of the QDs indicating that in the absence of Fermi

level pinning Au and Ag should form a favorable contact with the PbS layer. However, we have shown evidence for the formation of an unfavorable Schottky barrier with opposite polarity to the heterojunction diode. Therefore, we conclude that the metal/PbS interface undergoes Fermi level pinning, consistent with previous reports for PbSe QD Schottky junction solar cells.¹

The barrier height for a Schottky contact in the absence of Fermi level pinning is determined by the difference in the valence band edge and the metal Fermi energy (or metal work function). The band bending at the semiconductor–metal interface can be characterized by the difference in the valence band edge in the bulk layer and at the interface and is related to the barrier height. In the case of Fermi level pinning at the semiconductor/metal interface, the barrier height is related to the difference between the valence band edge and some characteristic energy level. As E_g increases, the Schottky barrier height increases, consistent with our measurements.

The V_{oc} in heterostructure devices is determined by the difference of the quasi-Fermi level of holes (E_{fp}) at the metal, hole extracting interface, and quasi-Fermi level of electrons (E_{fn}) at the n-type ZnO NC/ITO interface.³¹ Therefore the maximum V_{oc} is determined by the difference in the equilibrium junction potential. The realized V_{oc} is determined not only by the energetics but by the total recombination within the device. Recombination at the interfaces is likely a significant problem within this device structure and limits the V_{oc} .

The hole-injection barrier can be corrected by two strategies: the first is to choose a high work function metal such as Au. A high work function contact is required to minimize the hole-injection barrier; however, Fermi level pinning at the QD/metal interface prevents elimination of the barrier in the structures tested so far.

We have shown here that even with a work function that is larger than the Fermi level of the PbS layer, a Schottky barrier is formed that impedes hole-injection. This is likely due to Fermi level pinning at the PbS/Au interface. A second strategy invokes the establishment of a heavily p-doped surface layer in order to enable the tunneling of holes through the barrier height, which is not easy to achieve in our system but is the subject of future investigations and would lead to better behaved $J-V$ characteristics and corresponding higher conversion efficiencies.

In conclusion, the $J-V$ characteristics are investigated in a heterojunction PbS QD solar cell with structure of ITO/ZnO NC/PbS QD/metal and can be described by two opposing diodes: one formed by the ZnO/PbS interface and the other by the PbS/metal contact. The Schottky barrier height is a function of the QD band gap energy and back contact metal work function. We find that the Fermi levels are pinned at the metal/semiconductor junction and likely at the ZnO NC/PbS QD layer interface as well. Further work to understand and optimize the interfaces of these heterostructured QD solar cells should lead to an increase in power conversion efficiency. The recent demonstration of air stability⁷ combined with the potential for very high efficiencies³² motivates further investigation of QD solar cells.

■ ASSOCIATED CONTENT

S Supporting Information. Detailed information on materials, ZnO NCs, PbS QD synthesis, and methods used to fabricate and characterize devices, additional fitting parameters

used to model the $J-V$ curves, and a cross section SEM image of a typical device structure. This material is available free of charge via the Internet at <http://pubs.acs.org>.

■ AUTHOR INFORMATION

Corresponding Author

*E-mail: Matt.beard@nrel.gov.

■ ACKNOWLEDGMENT

The authors thank Mark Hanna, J. C. Johnson, J. van de Lagemaat, M. Reese, and A. Nardes for helpful discussions. We thank Bobby To for SEM imaging. J.G. and R.J.E. were supported by a PV seed fund provided by the NCPV program at NREL. J.M.L., O.E.S., A.J.N., and M.C.B. were supported by the Center for Advanced Photophysics an Energy Frontier Research Center funded by U.S. DOE Office of Science. The DOE work was funded by Contract DE-AC36-08GO28308 to NREL.

■ REFERENCES

- (1) Luther, J. M.; Law, M.; Beard, M. C.; Song, Q.; Reese, M. O.; Ellingson, R. J.; Nozik, A. J. *Nano Lett.* **2008**, *8*, 3488–3492.
- (2) Tang, J.; Wang, X.; Brzozowski, L.; Barkhouse, D. A. R.; Debnath, R.; Levina, L.; Sargent, E. H. *Adv. Mater.* **2010**, *22*, 1–5.
- (3) Johnston, K. W.; Pattantyus-Abraham, A. G.; Clifford, J. P.; Myrskog, S. H.; Hoogland, S.; Shukla, H.; Klem, E. J. D.; Sargent, E. H. *Appl. Phys. Lett.* **2008**, *92*, No. 122111.
- (4) Tang, J.; Brzozowski, L.; Barkhouse, D. A. R.; Wang, X.; Debnath, R.; Wolowicz, R.; Palmiano, E.; Levina, L.; Pattantyus-Abraham, A. G.; Jamakosmanovic, D.; Sargent, E. H. *ACS Nano* **2010**, *4*, 869–878.
- (5) Choi, J. J.; Lim, Y.; Santiago-Berrios, M. B.; Oh, M.; Hyun, B.; Sun, L.; Bartnik, A. C.; Goedhart, A.; Malliaras, G. G.; Abruña, H. D.; Wise, F. W.; Hanrath, T. *Nano Lett.* **2009**, *9*, 3749–3755.
- (6) Leschkie, K. S.; Beatty, T. J.; Kang, M. S.; Norris, D. J.; Aydil, E. S. *ACS Nano* **2009**, *3*, 3638–3648.
- (7) Luther, J. M.; Gao, J.; Lloyd, M. T.; Semonin, O. E.; Beard, M. C.; Nozik, A. J. *Adv. Mater.* **2010**, *22*, 3704–3707.
- (8) Pattantyus-Abraham, A. G.; Kramer, I. J.; Barkhouse, A. R.; Wang, X.; Konstantatos, G.; Debnath, R.; Levina, L.; Raabe, I.; Nazeeruddin, M. K.; Grätzel, M.; Sargent, E. H. *ACS Nano* **2010**, *4*, 3374–3380.
- (9) Ma, W.; Luther, J. M.; Zheng, H.; Wu, Y.; Alivisatos, A. P. *Nano Lett.* **2009**, *9*, 1699–1703.
- (10) Law, M.; Beard, M. C.; Choi, S.; Luther, J. M.; Hanna, M. C.; Nozik, A. J. *Nano Lett.* **2008**, *11*, 3904–3910.
- (11) Demtsu, S. H.; Sites, J. R. *Thin Solid Films* **2006**, *510*, 320–324.
- (12) Niemegeers, A.; Burgelman, M. J. *Appl. Phys.* **1997**, *81*, 2881–2886.
- (13) Godoy, A.; Cattin, L.; Toumi, L.; Diaz, F. R.; del Valle, M. A.; Soto, G. M.; Kouskoussa, B.; Morsli, M.; Benchouk, K.; Khelil, A.; Bernède, J. C. *Sol. Energy Mater. Sol. Cells* **2010**, *94*, 648–654.
- (14) Kouskoussa, B.; Morsli, M.; Benchouk, K.; Louarn, G.; Cattin, L.; Khelil, A.; Bernède, J. C. *Phys. Status Solidi A* **2009**, *206*, 311–315.
- (15) Gill, W. D.; Bube, R. H. *J. Appl. Phys.* **1970**, *41*, 3731.
- (16) Pfisterer, F. *Thin Solid Films* **2003**, *431*, 470.
- (17) Rothwarf, A. *Sol. Cells* **1980**, *2*, 115.
- (18) Green, M. A. *Solar Cells: Operating Principles, Technology, and System Applications*; Prentice-Hall: Englewood Cliffs, NJ, 1982.
- (19) Wu, Y.; Wadia, C.; Ma, W.; Sadtler, B.; Alivisatos, A. P. *Nano Lett.* **2008**, *8*, 2551–2555.
- (20) Jain, A.; Kapoor, A. *Sol. Energy Mater. Sol. Cells* **2005**, *86*, 197–205.
- (21) Mazhari, B. *Sol. Energy Mater. Sol. Cells* **2006**, *90*, 1021–1033.

- (22) Hyun, B. -B; Zhong, Y-W; Bartnik, A. C.; Sun, L.; Abruña, H. D.; Wise, F. W.; Goodreau, J. D.; Matthews, J. R.; Leslie, T. M.; Borrelli, N. F. *ACS Nano* **2008**, *11*, 2206–2212.
- (23) Pan, J; Gloeckler, M.; Sites, J. R. *J. Appl. Phys.* **2006**, *100*, 124505.
- (24) Kang, I.; Wise, F. W. *J. Opt. Soc. Am. B* **1997**, *14*, 1632–1646.
- (25) Wehrenberg, B. L.; Yu, D.; Ma, J.; Guyot-Sionnest, P. *J. Phys. Chem. B* **2005**, *109*, 20192–20199.
- (26) Luther, J. M.; Law, M.; Song, Q.; Perkins, C. L.; Beard, M. C.; Nozik, A. J. *ACS Nano* **2008**, *2*, 271–280.
- (27) Liu, Y.; Gibbs, M.; Puthussery, J.; Gaik, S.; Ihly, R.; Hillhouse, H. W.; Law, M. *Nano Lett.* **2010**, *10*, 1960–1969.
- (28) Sze, S. *Physics of Semiconductor Devices*, 2nd ed.; Wiley: New York, 1981.
- (29) Hyun, B.-R.; Zhong, Y.-W.; Bartnik, A. C.; Sun, L.; Abruña, H. D.; Wise, F. W.; Goodreau, J. D.; Matthews, J. R.; Leslie, T. M.; Borrelli, N. F. *ACS Nano* **2008**, *2*, 2206–2212.
- (30) Timp, B. A.; Zhu, X. Y. *Surf. Sci.* **2010**, *604*, 1335–1341.
- (31) Gregg, B. A.; Hanna, M. C. *J. Appl. Phys.* **2003**, *93*, 3605–3614.
- (32) Beard, M. C.; Midgett, A. G.; Hanna, M. C.; Luther, J. M.; Hughes, B. K.; Nozik, A. J. *Nano Lett.* **2010**, *10*, 3019–3027.